RSC Advances

Volume 1 | Number 1 | Jan 2013 | Pages 1–100

RSC Advances

www.rsc.org/advances

ROYAL SOCIETY OF CHEMISTRY

ROYAL SOCIETY OF CHEMISTRY

www.rsc.org/advances

Novel urchin-like Fe_2O_3@SiO_2@TiO_2 microparticles with magnetically separable and photocatalytic properties

Wai Szeto[1], Jiantao Li[2], Haibao Huang[1,3], Jin Xuan[4], Dennis Y.C. Leung[1]*

1. Department of Mechanical Engineering, The University of Hong Kong, Hong Kong, China.
2. FRIPP, China Petroleum & Chemical Corporation, Fushun, China.
3. School of Environmental Science and Engineering, Sun Yat-sen University, China.
4. School of Engineering and Physical Sciences, Heriot-Watt University, Edinburgh, U.K.

Abstract

Novel urchin-like microparticles with photocatalytic activity and magnetically separable property were prepared by a layer-by-layer assembly process. Photocatalytic degradation was investigated using 2 types of mercury vapor lamps: an ozone generating lamp emitting at both 254 nm and 185 nm as well as a germicidal lamp emitting at 254 nm only. This novel photocatalyst demonstrated superior photocatalytic activity in the mineralization of phenol under UVC illumination compared with the commercial P25, Degussa TiO_2, especially in repeated usage. Importantly, this photocatalyst can be quickly separated for reuse by simply using a magnet. The merits of 3D spiny nanostructured TiO_2 microparticle photocatalysts are high specific surface area, good permeability, reduced charge recombination rate and high catalytic activity while incorporation of magnetically separable property enables rapid and easy retrieval of suspended photocatalyst after use.

Keywords: Photocatalyst, Advanced oxidation, Core shell, Magnetic, Spiny

Table of contents/Abstract art

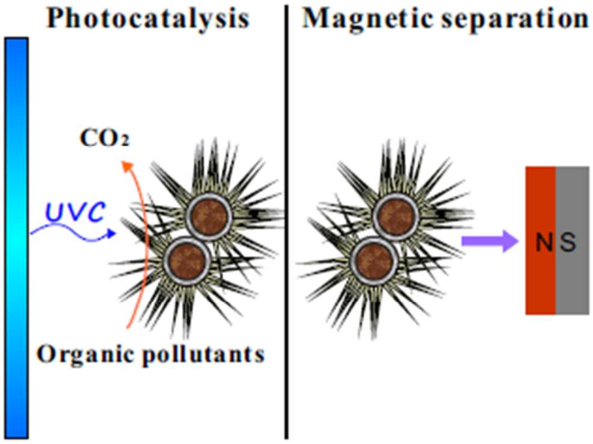

Novel 3D spiny nanostructured TiO_2 photocatalyst with γ-Fe_2O_3 core possesses good activity under UVC light, reusability and magnetically separable property.

Introduction

Industrial activities produce huge amount of organic pollutants.[1-5] Some of these pollutants pose serious threats to both the ecosystem and human being. Removal of these pollutants from waste streams is highly necessary, particularly under current's stringent regulation. For example, phenol is a representative organic pollutant that can be found with considerable amount in effluents of various industries such as petrochemical processes[3, 6], coal gasification[2] and steel production[7]. Moreover, phenol is a persistent organic pollutant[3], toxic even at very low concentration with high biorecalcitrance[8, 9]. Owing to the high solubility, satisfactory removal is difficult to attain with traditional treatments.[4] Therefore, much attention have been paid to advanced oxidation processes (AOPs), characterized by the in suite generation of highly reactive hydroxyl radical and capable to destroy some recalcitrant organic molecules, in the past few decades.[3] Heterogeneous photocatalysis employing semiconductor catalysts (TiO_2, ZnO, Fe_2O_3 and ZnS) is a promising technology among various AOPs. Owing to its low cost, low toxicity and high stability, as well as extremely impressive ability to decompose organic pollutants, TiO_2 becomes one of the most promising materials for the photocatalytic application in the environmental remediation aspect.[10] Nevertheless, there are still lots of room for improvement. Suppressing the recombination of the photo-generated holes and electrons and then enhancing the photodegradation efficiency by incorporating precious metals into TiO_2 has already been a classical example.[11-13] However, the limited supply and the rapidly booming price of precious metals have rendered this methodology impractical for environmental application. Suppression of charge recombination can also be achieved by merely morphological manipulations. 3D spiny TiO_2 nanostructures have higher specific surface area, more sharp corners as well as edges that serve as active sites for reaction,[14] higher permeability,[15] higher porosity, lower density, higher light-harvesting capacity,[16] and improved charge separation[17] compared with nanoparticles normally with diameters of 5-50 nm which have been extensively used. Photocatalysts are usually prepared in free nanoparticle form because of the high specific surface area. However, the difficult and costly post-treatment separation of nanoparticles from water is a severe problem restricting its industry utilization.[18] These burdens can be easily avoided if the photocatalyst is magnetically separable. Magnetically separable property can be obtained by inclusion of ferromagnetic and ferrimagnetic materials and oxides of iron (Fe_3O_4 and γ-Fe_2O_3) are convenient choices. However, this could reduce the photocatalytic activity of the original photocatalyst if heterojunction is formed[19, 20] because of the increased charge recombination rate.[18] Encapsulating the magnetic materials with SiO_2[18-20] can cope with the adverse effects of these materials because the SiO_2 can insulate the photocatalyst from the oxides of iron. The reported photocatalyst in this paper is an attempt to combine the two above-mentioned characteristics, namely 3D spiny nanostructure and magnetically separable property, together. Over the last few years, publications concerning photocatalysts with the iron oxide @ SiO_2 @ TiO_2 core-shell structures were not uncommon.[18, 21-23] Nevertheless, in most of these publications, the TiO_2 layer of photocatalysts did not have a featured morphology. To the best of our knowledge, only Su et al.[24] have reported a photocatalyst with interwoven TiO_2 nanopetals on surface and magnetic recyclability simultaneously. On the other hand, so far there is no report about magnetically separable photocatalysts with 3D spiny morphology. Here, a novel photocatalyst with urchin-like Fe_2O_3 @ SiO_2 @ TiO_2 microparticle morphology and magnetically separable property, namely magnetically separable spiny TiO_2 (MSST), has been developed and its photocatalytic efficiency of mineralizing phenol under UVC irradiation has been compared to that of the commercial P25, Degussa TiO_2.

Photocatalytic activities of photocatalysts in the related publications were usually assessed with UVA,[22, 25] artificial solar light[18] or visible light[23, 26, 27] and these photocatalysts may be aimed at working under solar light mainly. This may be due to the fact that sunlight is a free and sustainable resource. However, the uncontrollable and unreliable nature of weather may preclude the industrial application of the solar light based systems. In other words, use of artificial light sources may be necessary. When it comes to artificial light sources, there has been a broad agreement that shorter the light wavelength, the higher is the photodegradation efficiency.[28-31] Additionally, UVC is necessary for efficient mineralization of organic molecules.[32] Thus, more attention should be placed on UVC light sources. Low pressure mercury arc lamps, including classical mercury vapor lamps, amalgam lamps and microwave discharge electrodeless lamps, emitting mainly at 254 nm, are now commercially available and widely used in water disinfection, seem suitable for practical photocatalytic applications. Some of these lamps, constructed with high purity quartz and producing non-negligible light emission at 185 nm, are capable to generate ozone in air and hydroxyl radical (•OH) in water.[33] Use of ozone generating mercury arc lamps is not uncommon in the researches concerning gaseous state photocatalytic degradation but the same is not true for the photocatalytic degradation in aqueous state. As far as we know, only our research group has compared the photocatalytic degradation of dyes in aqueous state catalyzed by suspended TiO_2 using ozone generating mercury arc lamp emitting at both 185 nm and 254 nm (VUV lamp) and that using germicidal lamp emitting at 254 nm only (UV lamp).[34] Therefore, it is worth exploring the photocatalytic efficiencies of these UVC light sources in mineralizing phenol. In this study, classical mercury vapor lamp with VUV output was adopted as the light source primarily. To investigate the significances of the radiation at 185 nm, experiment using the lamp with UV output only was also performed.

Experimental

Materials

Anhydrous sodium acetate (NaAc), iron(III) chloride hexahydrate, polyethylene glycol (PEG) and tetraethyl orthosilicate (TEOS) were purchased from Aladdin reagents (Shanghai) Co. Ltd. Ethylene glycol and phenol were obtained from Oriental Chemicals & Lab supplies Ltd. Absolute ethanol, ammonia solution (33%), glycerol, sodium citrate dihydrate and tetrabutyl orthotitanate (TBOT) were purchased from Merck, Riedel-de Haen chemical, Fisher chemical, J&K chemical and

Shanghai Lingfeng chemical reagent CO. Ltd, respectively. All reagents were used as received without further purification. Barnstead Smart2pure UV water was used for solution preparation.

Preparation

Preparation of Fe_3O_4 nanospheres

The Fe_3O_4 particles were prepared via a solvothermal method as reported previously.[35] 28.8 g of NaAc, 10.8 g of iron(III) chloride hexahydrate, 8 g of PEG, 5.76 g of sodium citrate dihydrate and 320 ml of ethylene glycol were mixed together and stirred vigorously for 30 minutes. The mixture was transferred to a teflon lined stainless-steel autoclave with 500 ml capacity and 8 hours of heating at 200 °C was applied. The black precipitate formed was separated from the mother liquor by centrifugation and washed with water thrice and with ethanol twice, followed by magnetic separation. The nanospheres were finally dried at 60 °C under helium atmosphere for 6 hours.

Fabrication of SiO_2 coated Fe_3O_4 nanospheres (Fe_3O_4 @ SiO_2)

The Fe_3O_4 nanospheres were coated with amorphous SiO_2 via a modified stöber method. The first step of coating procedure was dispersing 0.25 g of the Fe_3O_4 nanospheres in 30 ml water with ultrasonication and shaking. 30 ml of ethanol and 5 ml of ammonia solution were added to the suspension under further ultrasonication. A solution consisting 1 ml of TEOS and 30 ml of ethanol was poured into the suspension under further ultrasonication. The reaction was allowed to proceed for 2 hours under continuous ultrasonication and intermittent shaking. The resultant precipitate was collected by magnetic separation and washed with water thrice and with ethanol twice, followed by drying at 60 °C for 6 hours.

Fabrication of MSST

The nano-spiny TiO_2 was planted onto the Fe_3O_4 @ SiO_2 through a modified solvothermal process reported by Tian et al.[15] with subsequent calcination. Typically, 0.223 g of Fe_3O_4 @ SiO_2 was ultrasonically dispersed into 30 ml of ethanol in a 100 ml autoclave lining. 12.6 g of glycerol was added into the suspension followed by vigorous stirring and ultrasonication. 2 ml of TBOT was dropped into the above mixture and subsequent vigorous stirring and ultrasonication were applied. 12 hours of heating at 180 °C was applied to allow the reaction to occur. The black precipitate formed was separated from the mother liquor by filtering with a buchner funnel with suction and washed with ethanol 4 times, followed by drying at 60 °C for 3 hours. In order to convert the formed organic precursor of TiO_2 into anatase phase, the dried precipitate was calcinated at 450 °C for 3 hours started with a heating rate of 7 °C/min. The Fe_3O_4 cores were oxidized to γ-Fe_2O_3 during the calcination.

Characterization

To characterize the size and morphology of the samples, images of transmission electron microscopy (TEM; Philips CM100, 100 kV) and scanning electron microscopy (FESEM; Leo 1530, 5 kV) were acquired. The distribution of elements in the sample microparticles was visualized with the transmission electron microscopy (TEM; FEI Tecnai G2 20, 200 kV) with attached energy dispersive X-ray spectroscopy (EDX). Powder X-ray diffraction (XRD) patterns were taken to characterize the crystal structures inside the samples on a Bruker AXS D8 Advance X-ray diffractometer. Measurement was performed with Cu Kα radiation (λ = 1.54 Å) in the range of 2θ = 20-90°. The scanning speed, tube voltage and anode current were 6 °/min, 40kV and 40mA, respectively.

Measurement of photocatalytic activity

The photocatalytic activities of the prepared samples in mineralizing phenol were evaluated at ambient temperature. In a typical test, a certain amount of photocatalyst containing 0.16 g of TiO_2 was dispersed ultrasonically in 152 ml of water and then 8 ml of 1000 mg/L phenol solution was added into the suspension so that the initial phenol concentration was 50 ppm, the initial chemical oxygen demand (COD), due to phenol, of the solution was 120 mg/L and the TiO_2 dosage was 1 g/L; considering that 0.611 g of MSST photocatalyst was obtained in a typical preparation with 0.223 g of inert template, the TiO_2 loading of MSST was 64% and the experiments involving MSST were carried out with 0.250 g of photocatalyst composite so that the TiO_2 dosage was 1 g/L eventually. The mixture was transferred to a cylindrical glass photoreactor shown in figure 1 with height of 220 mm, inner diameter of 42 mm and effective volume of 160 mL. A lamp with waterproof quartz sleeve was placed coaxially inside the photoreactor. Continuous air purging at 0.3 L/min was applied to provide oxygen and agitation. Before switching on the VUV lamp, air purging was applied for 3 minutes. The duration of illumination was 1 hour and the lamp used was a hot cathode low pressure mercury vapor lamp with VUV output (10 W, U-VIX brand, ZW10D15Y). 2.5 ml of sample was withdrawn from the reaction mixture every 10 minutes. The suspended photocatalyst was retrieved from the suspension by applying a magnetic field whenever possible or centrifugation. The extent of mineralization of phenol was monitored by COD analysis using Hach method 8000 with low range digestion vials. The recyclability of the photocatalysts was assessed by repeating the above photocatalytic activity test with the catalyst retrieved and the catalyst was rinsed with water once before the subsequent experiment. The cycle of test was repeated up to six times. For comparison purposes, an experiment was carried out with another UV lamp (10 W, U-VIX brand, ZW10D15W) without VUV output.

Results and discussion

TEM, EDX and SEM

TEM images of the materials acquired from different stages of the preparation of the photocatalyst, with 12 hours of solvothermal process, were shown in figure 2. As shown in figure 2a, the prepared Fe_3O_4 nanospheres with diameters of ~280 nm were characterized by rough surface. After the Stöber process, a layer of SiO_2 coating with relatively smooth surface and an average thickness of 44 nm was found on the Fe_3O_4 nanospheres while the spherical morphology was maintained (figure 2b and S3 of supporting Information). The final material, i.e. the MSST photocatalyst, with urchin-like appearance and spiny surface morphology as revealed in figure 2c was obtained after the 12 hour solvothermal process with subsequent calcination. Inside the outermost spiny layer of TiO_2, coalescence of γ-Fe_2O_3 @ SiO_2 templates occurred. It seemed that multiple γ-Fe_2O_3 @ SiO_2 nanospheres agglomerated together to form micron sized lumps during the early stages of the solvothermal process. In other words, micron sized lumps of Fe_3O_4 @ SiO_2 nanospheres formed before the formation of spiny structure. Depicted in figure 2d, within the cluster of nanospheres enclosed by the TiO_2 shell, spiny material was seldom observed between the γ-Fe_2O_3 @ SiO_2 nanospheres. The evolution of this 3D hierarchical spiny structure in template-free condition has been described by Tian et al.[15] and consisted of initial formation of interconnected sphere-like microparticles and the subsequent dissolution-recrystallization growth that formed the spines. In the situation presented in this article, heterogeneous nucleation of the transformation from the miscible titanium species to the precipitated material on the surface of the templates, namely Fe_3O_4 @ SiO_2 nanospheres, could occur at the initial stages of the solvothermal process. Similar to the template-free condition that the initially precipitated material had tendency to become interconnected, the same phenomenon would also happen to precipitated material with encapsulated Fe_3O_4 @ SiO_2 nanospheres so that grape-like micron sized clusters were formed. As the reaction proceeded, dissolution-recrystallization growth of the spiny material took place on the outer surface of the micron sized clusters. Finally, a photocatalyst with unusual urchin-like core-shell architecture was obtained. Elemental mapping of O, Si, Ti and Fe on the MSST photocatalyst was carried out with EDX (figure 2e). A double-shelled structure with TiO_2 outermost shell and iron oxide core with sandwiched SiO_2 layer has been successfully fabricated. SEM images of the calcinated MSST photocatalyst synthesized with 3, 6, 12, 18 and 24 hours of solvothermal process were also obtained (figure S1a – e, supporting information). One can see that the stings on surface were not yet fully developed until the time of the solvothermal reaction reached 12 hours and the morphological evolution seemed halted later on. The SEM image of the material with 3 hours of solvothermal reaction showed that the nano-sized spheres were already agglomerated and buried in the titanium disposition. This again suggested that the micron sized lumps of Fe_3O_4 @ SiO_2 nanospheres formed before the formation of the spiny structure.

XRD analysis

As shown in figure 3, the crystalline phases of the prepared MSST photocatalysts with different durations of solvothermal process (i.e. 3, 6, 12, 18 and 24 hours) were analyzed with XRD. Characteristic peaks of anatase TiO_2 (PDF 84-1285, at 2θ = 25.3, 37.9, 48.0, 54.0, 55.0, 62.8, 68, 70.4, 75.1 and 82.7 °) and γ-Fe_2O_3 (PDF 39-1346 at 2θ = 30.2, 35.7, 43.4 and 57.2 °) can be clearly identified in the XRD patterns of all the 5 samples. At 2θ = 27.5 °, a barely detectable peak possibly caused by the presence of trace rutile TiO_2 was also found in the XRD patterns of the samples with 6 - 24 hours of solvothermal process. The extent of broadening of the peaks related to anatase increased with the duration of the solvothermal process. According to the Scherrer equation, the average crystalline sizes of anatase phase in the samples were estimated using the full-width-half-maximum (FWHM) of the peak with the greatest intensity at 2θ = 25.3 ° and the results were presented on table 1. An interesting phenomenon that the crystalline size of anatase decreased with increasing time of solvothermal process was demonstrated. Despite of the fact that the anatase phase was formed during the calcination at 450 °C after the solvothermal process,[15] the crystal structure of the final product depended on the condition of the solvothermal process.

Photocatalytic activity

The photocatalytic performances of the prepared MSST samples were evaluated by conducting photocatalytic mineralization test on phenol. In order to investigate the effect of duration of the solvothermal process, the MSST photocatalysts with different solvothermal times (3, 6, 12, 18 and 24 hours) were prepared and tested. Experiment using commercial P25 TiO_2 was carried out for comparison. As shown in figure 4, phenol can be mineralized under the illumination of such an energetic VUV light in the absence of photocatalyst and full mineralization occurred after 95 minutes of illumination (shown in the next graph). Nevertheless, about 2 times faster mineralization can be achieved in the system with the photocatalysts and the best one had the mineralization completed within 42 minutes. The catalytic efficiency followed the order of MSST (6 or 12 hours of solvothermal process) > MSST (18 hours of solvothermal process) > MSST (3 or 24 hours of solvothermal process) > P25. Obviously, this micron sized MSST photocatalyst outperformed the P25 nanoparticles having a much smaller average particle size of 21 nm. The good photocatalytic activity of the MSST photocatalyst may be explained by its special morphology of the surface TiO_2 which resulted in enhanced charge separation, increased mass transfer, larger surface area and more active sites for reactions to take place. The most likely explanation of the inferior photocatalytic activity of the MSST with 3 hours of solvothermal process was that the nano-spiny TiO_2 structure was not yet developed. The relatively weak performance of MSST with solvothermal processing time longer than 12 hours would be due to the large number of surface defects and recombination centers.[36] Referring to the result of XRD analysis, the longer the solvothermal processing, the smaller was the crystalline size of the anatase. A possible explanation for this was increased loading of impurity. For this system, the most likely impurity was carbon. It has been reported that introduction of various impurities including carbon into TiO_2 can decrease the crystalline size after calcination.[37-42] Doped TiO_2 usually possesses good visible light photocatalytic activity yet it is generally weak under UV light.[43-46] In the absence of UV light, the control experiment carried out with MSST with 12 hours of solvothermal process demonstrated that there was no adsorption of phenol onto this photocatalyst. MSST with 12 hours of solvothermal process was selected for the subsequent experiments because it showed good photocatalytic activity accompanied by fully developed nano-spiny morphology.

Significance of photocatalyst and comparison of the mercury vapor lamps

As shown in figure 5, the photocatalytic mineralization plots, i.e. COD vs time plots, were essentially linear in the presence of the MSST photocatalyst until the degree of mineralization was high especially for the VUV + MSST condition. In other words, the kinetics of mineralization was zero-order in COD. Afterwards, the mineralization rate started to be dependent on remaining COD or degree of mineralization. This phenomenon has been discussed elsewhere.[47] Briefly, in an AOP, concentration of radical species responsible for oxidation is unchanged in steady state and if the concentration of a material to be oxidized is high, the mineralization rate of this material will be proportional to the rate of radical generation only. However, if the concentration of the material becomes low, its concentration becomes important as competitive scavenging reactions become increasingly significant. Thus, transition of reaction kinetics is possible if the initial concentration of the material to be oxidized is high accompanied by high eventual degree of removal. In the experiments presented in this work carried out with impurity free solution, the competitive reaction could be various charge recombination reactions.[48, 49] The photolytic mineralization in the absence of photocatalyst under VUV light also demonstrated complex kinetic behavior while that under UV light showed 1st order kinetics with respect to COD and the rate constant was determined to be 0.239 h^{-1}. A calculated profile of VUV + MSST experiment, based on the assumption that in the VUV + MSST experiment, the overall mineralization was owing to the parallel reactions of the VUV photolysis and the UV + MSST photocatalysis and evaluated by the equation (1) below, was also included for discussion.

$$\frac{dCOD}{dt_{overall}} = \frac{dCOD}{dt_{UV+MSST}} + \frac{dCOD}{dt_{VUV}} - \frac{dCOD}{dt_{UV}} \quad (1)$$

Where

$\frac{dCOD}{dt_{overall}}$ = The calculated mineralization rate of the of the VUV + MSST experiment

$\frac{dCOD}{dt_{UV+MSST}}$ = The COD dependent mineralization rate of the UV + MSST experiment

$\frac{dCOD}{dt_{VUV}}$ = The COD dependent mineralization rate of the VUV only experiment

$\frac{dCOD}{dt_{UV}}$ = The COD dependent mineralization rate of the UV only experiment

In order to compare the efficiencies of the four aforementioned experiments with disparate kinetic behaviors, a simple figure-of-merit based on electric energy consumption as defined by Bolton et al.[47] can be useful and informative. This is further justified by the fact that the main operating expense of photocatalytic degradation comes from electricity. The appropriate figure-of-merit, for the cases that the kinetics is phenomenologically zero-order in COD, is the electric energy per mass (E_{EM}) defined as:

$$E_{EM} = \frac{Pt10^6}{V(\gamma_i - \gamma_f)} \quad (2)$$

Where P is the rated power (kW) of the system, V is the volume (L) of water treated in time t (h), γ_i and γ_f are the initial and final COD (mg/L), and the factor of 10^6 converts mg to kg.

Lower E_{EM} values (in kwh/kg COD) correspond to more economical removal. Electric energy per order, designated for the 1st order reactions, was not adopted as complete COD removal was observed in most of the experiments and these experiments were obviously not the 1st order reaction. Referring to the plots, the E_{EM} values of complete COD removal were listed on table 2. As shown in table 2, the E_{EM} of the photolysis with VUV light only was 2.26 times larger than that of photocatalytic degradation in presence of MSST photocatalyst; using this photocatalyst, 56% of electricity cost of the aforementioned mineralization process can be cut. Thus, the MSST photocatalyst was obviously effective. The huge ratio of E_{EM} values between the photocatalytic and photolytic experiments using UV lamp implied that the photocatalytic degradation was much more important than the photolysis under the 254 nm radiation. Comparing the E_{EM} of photocatalytic degradation experiments in presence of MSST photocatalyst, VUV lamp was 43% more energetically efficient than the UV lamp. Moreover, the photocatalytic mineralization under UV light showed higher COD concentration dependence compared to the corresponding experiment using VUV lamp. For removing 1st half of COD (i.e. from 120 to 60 mg/L), 20.7 and 23.7 minutes were needed for VUV lamp and UV lamp, respectively; using VUV lamp, the reaction rate was only 14.5% higher compared to using UV lamp. The corresponding values for removing 2nd half of COD (i.e. from 60 to 0 mg/L) were 21.3 and 36.3 minutes; using VUV lamp, the reaction rate was 70.4% higher than that of using UV lamp; unlike the VUV lamp which showed relatively steady reaction rate throughout the course of mineralization, UV lamp demonstrated a remarkably reduced rate of reaction in advancing mineralization. A possible explanation is the concentration dependence of the adsorption of organic materials onto photocatalyst surface; lower concentration resulted in reduced surface coverage so that the photogenerated holes and hydroxyl radicals on the surface would have less chance of oxidizing the organic materials before undergoing charge recombination.[48, 49] On the other hand, the photolytic mineralization under VUV light was mainly caused by hydroxyl radicals generated from photolysis of water[33] in bulk and suffered less from the low concentration of organic materials. Hence, the steady reaction rate of the VUV + MSST experiment would be due to the aid of photolysis caused by VUV light. This was also supported by the nearly constant mineralization rate of the VUV photolysis experiment in which the 1st and 2nd half of COD were removed in 48.3 and 46.7 minutes, respectively. Nevertheless, the rate of the actual VUV + MSST experiment was found slower than that of the aforementioned calculated profile, which had an 8.2% lower E_{EM}, shown in figure 5. Based on the aforementioned findings, it seemed that (1) there was no appreciable synergy between the 185 nm and 254 nm light, (2) the advantage of VUV lamp over UV lamp in photocatalytic mineralization was the comparatively higher mineralization rate and this became more notable with advancing COD removal, (3) benefited from the effective photolytic degradation provided by the VUV light, the rate of mineralization in the VUV + MSST experiment in high degree of COD removal was relatively steady.

Magnetic separation and recyclability of the photocatalyst

Figure 6 shows the results of repeated (i.e. 6 cycles) photocatalytic phenol mineralization catalyzed by the MSST (with 12 hours of solvothermal process) and the P25. The MSST was generally stable throughout the 6 cycles; no remarkable change in the rate of mineralization was observed. The same was not true for the P25. At the first time of use, 100% mineralization was attained within 60 minutes. This figure dropped gradually throughout the 6 cycles and finally reduced to 81%. For the 40 minute data, the trend was even more apparent. Besides, as shown in figure 7, the dispersed MSST can be separated from water within 5 minutes under a magnetic field generated by a small magnet while a high speed centrifuge was required for separating the P25 nanoparticles owing to its slow gravitational settling. These showed that the MSST photocatalyst was much more durable than the commercial P25 TiO_2 which was deactivated quickly within several cycles of use and using the MSST was very convenient as it can settle quickly under magnetic field after use.

Acknowledgement

The funding provided by China Petrochemical Technology Company Limited (Sinopec) is grateful acknowledged.

Reference

1. Coelho, A.; Castro, A. V.; Dezotti, M., Treatment of petroleum refinery sourwater by advanced oxidation processes. *J. Hazard. Mater.* **2006,** *137*, (1), 178-184.
2. Wang, W.; Han, H.; Yuan, M.; Li, H.; Fang, F.; Wang, K., Treatment of coal gasification wastewater by a two-continuous UASB system with step-feed for COD and phenols removal. *Bioresour. Technol.* **2011,** *102*, (9), 5454-5460.
3. Shahrezaei, F.; Mansouri, Y.; Zinatizadeh, A. A. L.; Akhbari, A., Process modeling and kinetic evaluation of petroleum refinery wastewater treatment in a photocatalytic reactor using TiO_2 nanoparticles. *Powder Technol.* **2012,** *221*, 203-212.
4. Wang, F.; Hu, Y.; Guo, C.; Huang, W.; Liu, C.-Z., Enhanced phenol degradation in coking wastewater by immobilized laccase on magnetic mesoporous silica nanoparticles in a magnetically stabilized fluidized bed. *Bioresour. Technol.* **2012,** *110*, 120-124.

5. Tran, B. C.; Teil, M. J.; Blanchard, M.; Alliot, F.; Chevreuil, M., BPA and phthalate fate in a sewage network and an elementary river of France. Influence of hydroclimatic conditions. *Chemosphere* **2015,** *119*, 43-51.

6. Lin, Y.-T.; Liang, C.; Chen, J.-H., Feasibility study of ultraviolet activated persulfate oxidation of phenol. *Chemosphere* **2011,** *82*, (8), 1168-1172.

7. Vazquez, I.; Rodrıguez, J.; Maranon, E.; Castrillon, L.; Fernandez, Y., Simultaneous removal of phenol, ammonium and thiocyanate from coke wastewater by aerobic biodegradation. *J. Hazard. Mater.* **2006,** *137*, (3), 1773-1780.

8. Ahmed, S.; Rasul, M.; Martens, W. N.; Brown, R.; Hashib, M., Heterogeneous photocatalytic degradation of phenols in wastewater: a review on current status and developments. *Desalination* **2010,** *261*, (1), 3-18.

9. Hasan, D. u. B.; Aziz, A.; Daud, M., Application of response surface methodology in process parameters optimization for phenol mineralization using Fenton's peroxidation. *Afr. J. Biotechnol.* **2013,** *10*, (50), 10218-10231.

10. Li, J. Y.; Cao, T. P.; Shao, C. L.; Wang, C. H., Preparation and Photocatalytic Properties of γ-Bi_2O_3/TiO_2 Composite Fibers. *Chinese Journal of Inorganic Materials* **2012,** *27*, 687-692.

11. Zhang, C.; He, H.; Tanaka, K.-i., Catalytic performance and mechanism of a Pt/TiO_2 catalyst for the oxidation of formaldehyde at room temperature. *Appl. Catal., B* **2006,** *65*, (1), 37-43.

12. Zhao, W.; Chen, C.; Li, X.; Zhao, J.; Hidaka, H.; Serpone, N., Photodegradation of sulforhodamine-B dye in platinized titania dispersions under visible light irradiation: influence of platinum as a functional co-catalyst. *J. Phys. Chem. B* **2002,** *106*, (19), 5022-5028.

13. Li, F.; Li, X., The enhancement of photodegradation efficiency using Pt-TiO_2 catalyst. *Chemosphere* **2002,** *48*, (10), 1103-1111.

14. Sun, Z.; Kim, J. H.; Zhao, Y.; Bijarbooneh, F.; Malgras, V.; Lee, Y.; Kang, Y.-M.; Dou, S. X., Rational design of 3D dendritic TiO_2 nanostructures with favorable architectures. *J. Am. Chem. Soc.* **2011,** *133*, (48), 19314-19317.

15. Tian, G.; Chen, Y.; Zhou, W.; Pan, K.; Tian, C.; Huang, X.-R.; Fu, H., 3D hierarchical flower-like TiO_2 nanostructure: morphology control and its photocatalytic property. *CrystEngComm* **2011,** *13*, (8), 2994-3000.

16. Song, H. J.; Chen, T.; Sun, Y. L.; Zhang, X. Q.; Jia, X. H., Controlled synthesis of porous flower-like TiO_2 nanostructure with enhanced photocatalytic activity. *Ceram. Int.* **2014,** *40*, 11015-11022.

17. Bai, H.; Liu, L.; Liu, Z.; Sun, D. D., Hierarchical 3D dendritic TiO_2 nanospheres building with ultralong 1D nanoribbon/wires for high performance concurrent photocatalytic membrane water purification. *Water Res.* **2013,** *47*, (12), 4126-4138.

18. Yu, X.; Liu, S.; Yu, J., Superparamagnetic γ-$Fe_2O_3@SiO_2@TiO_2$ composite microspheres with superior photocatalytic properties. *Appl. Catal., B* **2011,** *104*, (1-2), 12-20.

19. Chen, F.; Xie, Y.; Zhao, J.; Lu, G., Photocatalytic degradation of dyes on a magnetically

separated photocatalyst under visible and UV irradiation. *Chemosphere* **2001,** *44*, (5), 1159-1168.

20. Gao, Y.; Chen, B.; Li, H.; Ma, Y., Preparation and characterization of a magnetically separated photocatalyst and its catalytic properties. *Mater. Chem. Phys.* **2003,** *80*, (1), 348-355.

21. He, M.; DI, L.; Jiang, D.; Chen, M., Magnetically separable γ-Fe_2O_3@SiO_2@Ce-doped TiO_2 core-shell nanocomposites: Fabrication and visible-light-driven photocatalytic activity. *J. Solid State Chem.* **2012,** *192*, 139-143.

22. Cheng, J.; Ma, R.; Li, M.; Wu, J.; Liu, F.; Zhang, X., Anatase nanocrystals coating on silica-coated magnetite: Role of polyacrylic acid treatment and its photocatalytic properties. *Chem. Eng. J.* **2012,** *210*, 80-86.

23. Wu, S.-H.; Wu, J.-L.; Jia, S.-Y.; Chang, Q.-W.; Ren, H.-T.; Liu, Y., Cobalt (II) phthalocyanine-sensitized hollow Fe_3O_4@ SiO_2@ TiO_2 hierarchical nanostructures: Fabrication and enhanced photocatalytic properties. *Appl. Surf. Sci.* **2013,** *287*, 389-396.

24. Su, J.; Zhang, Y.; Xu, S.; Wang, S.; Ding, H.; Pan, S.; Wang, G.; Li, G.; Zhao, H., Highly efficient and recyclable triple-shelled Ag@Fe_3O_4@SiO_2@TiO_2 photocatalysts for degradation of organic pollutants and reduction of hexavalent chromium ions. *Nanoscale* **2014,** *6*, (10), 5181-5192.

25. Fu, W.; Yang, H.; Chang, L.; Li, M.; Zou, G., Anatase TiO_2 nanolayer coating on strontium ferrite nanoparticles for magnetic photocatalyst. *Colloids Surf., A* **2006,** *289*, (1), 47-52.

26. Amarjargal, A.; Jiang, Z.; Tijing, L. D.; Park, C.-H.; Im, I.-T.; CHEOL, S. K., Nanosheet-based α-Fe_2O_3 hierarchical structure decorated with TiO_2 nanospheres via a simple one-pot route: Magnetically recyclable photocatalysts. *J. Alloys Compd.* **2013,** *580*, 143-147.

27. Liu, Z.; Liu, X. Z.; Lu, D. Z.; Fang, P. F.; Wang, S. J., Grape-like Bi_2WO_6/TiO_2 hierarchical microspheres: A superior visible light photocatalyst with magnetic recycling property. *Mater. Lett.* **2014,** *130*, 143-145.

28. Ravichandran, L.; Selvam, K.; Swaminathan, M., Highly efficient activated carbon loaded TiO_2 for photo defluoridation of pentafluorobenzoic acid. *J. Mol. Catal. A: Chem.* **2010,** *317*, (1), 89-96.

29. Chang, C.-P.; Lu, M.-C., Effect of ferric ions on the photocatalytic oxidation of 2-chlorophenol with 254 and 365 nm UV lights. *J. Environ. Eng. Manage.* **2007,** *17*, (4), 235.

30. Bessekhouad, Y.; Robert, D.; Weber, J., Bi_2S_3/TiO_2 and CdS/TiO_2 heterojunctions as an available configuration for photocatalytic degradation of organic pollutant. *J. Photochem. Photobiol., A* **2004,** *163*, (3), 569-580.

31. Matthews, R. W.; McEvoy, S. R., A comparison of 254 nm and 350 nm excitation of TiO_2 in simple photocatalytic reactors. *J. Photochem. Photobiol., A* **1992,** *66*, (3), 355-366.

32. Li Puma, G.; Yue, P. L., Enhanced photocatalysis in a pilot laminar falling film slurry reactor. *Ind. Eng. Chem. Res.* **1999,** *38*, (9), 3246-3254.

33. Gonzalez, M. G.; Oliveros, E.; Wörner, M.; Braun, A. M., Vacuum-ultraviolet photolysis of aqueous reaction systems. *J. Photochem. Photobiol., C* **2004,** *5*, (3), 225-246.

34. Huang, H.; Leung, D. Y.; Kwong, P. C.; Xiong, J.; Zhang, L., Enhanced photocatalytic degradation of methylene blue under vacuum ultraviolet irradiation. *Catal. Today* **2013,** *201*,

189-194.

35. Deng, H.; Li, X.; Peng, Q.; Wang, X.; Chen, J.; Li, Y., Monodisperse Magnetic Single-Crystal Ferrite Microspheres. *Angew. Chem.* **2005,** *117*, (18), 2842-2845.

36. Wu, W.-Q.; Lei, B.-X.; Rao, H.-S.; Xu, Y.-F.; Wang, Y.-F.; Su, C.-Y.; Kuang, D.-B., Hydrothermal Fabrication of Hierarchically Anatase TiO_2 Nanowire arrays on FTO Glass for Dye-sensitized Solar Cells. *Sci. Rep.* **2013,** *3*.

37. Bhosale, R. R.; Pujari, S. R.; Muley, G. G.; Patil, S. H.; Patil, K. R.; Shaikh, M. F.; Gambhire, A. B., Solar photocatalytic degradation of methylene blue using doped TiO_2 nanoparticles. *Sol. Energy* **2014,** *103*, 473-479.

38. Galenda, A.; Crociani, L.; El Habra, N.; Favaro, M.; Natile, M. M.; Rossetto, G., Effect of reaction conditions on methyl red degradation mediated by boron and nitrogen doped TiO_2. *Appl. Surf. Sci.* **2014,** *314*, 919-930.

39. Gurkan, Y. Y.; Turkten, N.; Hatipoglu, A.; Cinar, Z., Photocatalytic degradation of cefazolin over N-doped TiO_2 under UV and sunlight irradiation: prediction of the reaction paths via conceptual DFT. *Chem. Eng. J.* **2012,** *184*, 113-124.

40. Li, X.; Liu, P. W.; Mao, Y.; Xing, M. Y.; Zhang, J. L., Preparation of homogeneous nitrogen-doped mesoporous TiO_2 spheres with enhanced visible-light photocatalysis. *Appl. Catal., B* **2015,** *164*, 352-359.

41. Nahar, M. S.; Zhang, J.; Hasegawa, K.; Kagaya, S.; Kuroda, S., Phase transformation of anatase–rutile crystals in doped and undoped TiO_2 particles obtained by the oxidation of polycrystalline sulfide. *Mater. Sci. Semicond. Process.* **2009,** *12*, (4), 168-174.

42. Bessekhouad, Y.; Robert, D.; Weber, J.-V.; Chaoui, N., Effect of alkaline-doped TiO_2 on photocatalytic efficiency. *J. Photochem. Photobiol., A* **2004,** *167*, (1), 49-57.

43. Manassero, A.; Satuf, M. L.; Alfano, O. M., Evaluation of UV and visible light activity of TiO_2 catalysts for water remediation. *Chem. Eng. J.* **2013,** *225*, 378-386.

44. Triantis, T. M.; Fotiou, T.; Kaloudis, T.; Kontos, A. G.; Falaras, P.; Dionysiou, D. D.; Pelaez, M.; Hiskia, A., Photocatalytic degradation and mineralization of microcystin-LR under UV-A, solar and visible light using nanostructured nitrogen doped TiO_2. *J. Hazard. Mater.* **2012,** *211*, 196-202.

45. Fotiou, T.; Triantis, T. M.; Kaloudis, T.; Hiskia, A., Evaluation of the photocatalytic activity of TiO_2 based catalysts for the degradation and mineralization of cyanobacterial toxins and water off-odor compounds under UV-A, solar and visible light. *Chem. Eng. J.* **2015,** *261*, 17-26.

46. Chen, K.; Li, J.; Li, J.; Zhang, Y.; Wang, W., Synthesis and characterization of TiO_2–montmorillonites doped with vanadium and/or carbon and their application for the photodegradation of sulphorhodamine B under UV–vis irradiation. *Colloids Surf., A* **2010,** *360*, (1), 47-56.

47. Bolton, J. R.; Bircher, K. G.; Tumas, W.; Tolman, C. A., Figures-of-merit for the technical development and application of advanced oxidation technologies for both electric-and solar-driven systems (IUPAC Technical Report). *Pure Appl. Chem.* **2001,** *73*, (4), 627-637.

48. Mohamed, H. H.; Bahnemann, D. W., The role of electron transfer in photocatalysis: Fact and

fictions. *Appl. Catal., B* **2012,** *128*, 91-104.

49. Liu, B.; Zhao, X., A kinetic model for evaluating the dependence of the quantum yield of nano-TiO_2 based photocatalysis on light intensity, grain size, carrier lifetime, and minority carrier diffusion coefficient: Indirect interfacial charge transfer. *Electrochim. Acta* **2010,** *55*, (12), 4062-4070.

The captions of Figures and Tables

Figure 1 The cylindrical glass photoreactor with light source

Figure 2 Electron microscopy images: (a) TEM of the Fe_3O_4 nanospheres; (b) TEM of the Fe_3O_4 @ SiO_2; (c) & (d) TEM of the MSST photocatalyst; (e) elemental mapping of the MSST

Figure 3 XRD patterns of MSST with different durations of the solvothermal process

Figure 4 Mineralization in presence of various photocatalysts

Figure 5 Mineralization in various conditions

Figure 6 Recyclability test of MSST and P25

Figure 7 Magnetic separation of MSST and gravitational settling of P25

Table 1 Estimated crystalline sizes of MSST with different durations of the solvothermal process

Table 2 E_{EM} values of various experiments

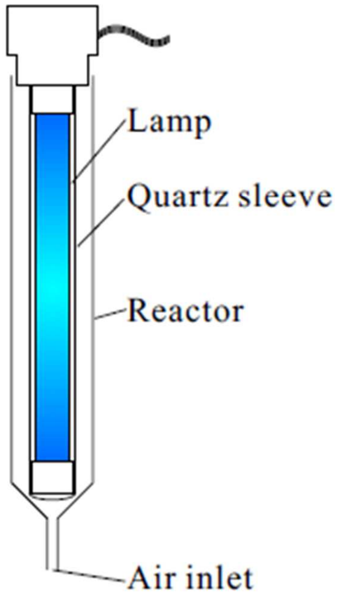

Figure 1

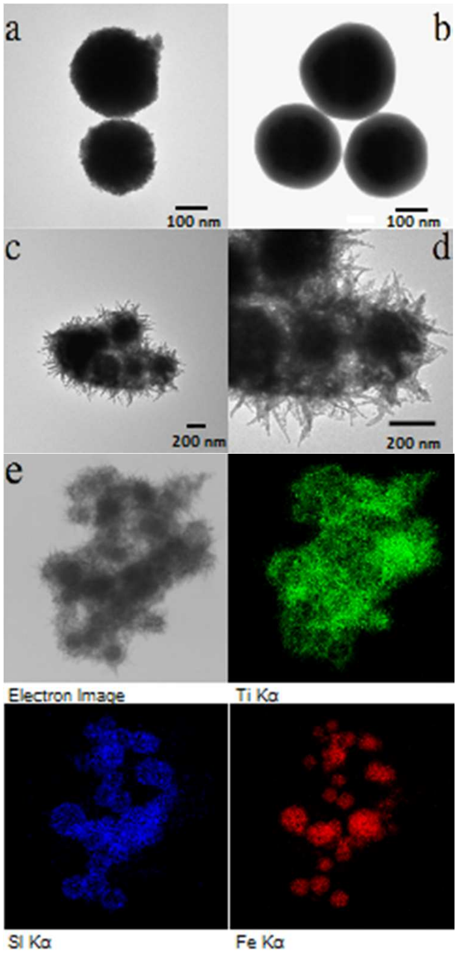

Figure 2

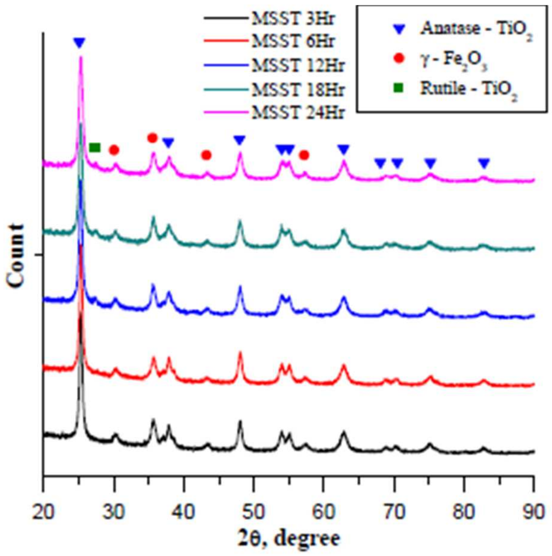

Figure 3

493

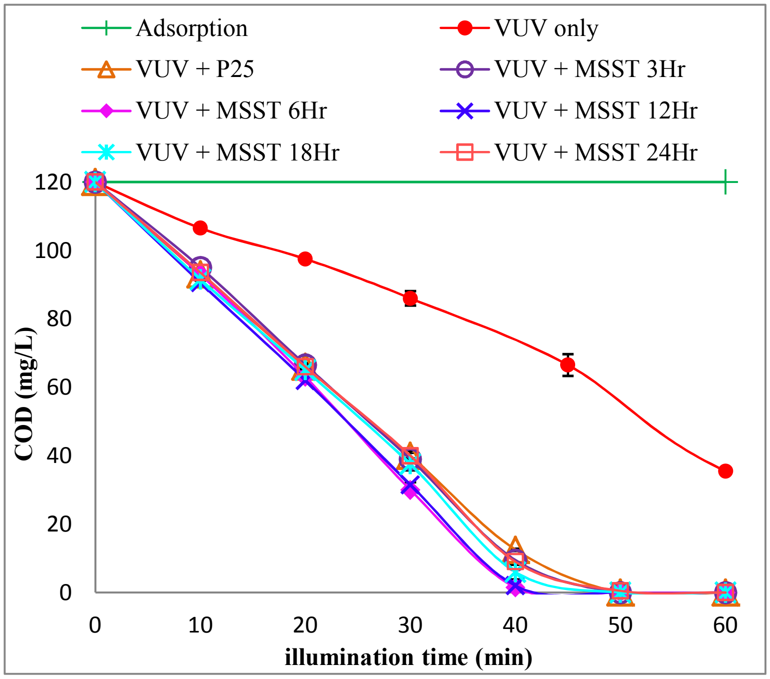

Figure 4

494

495

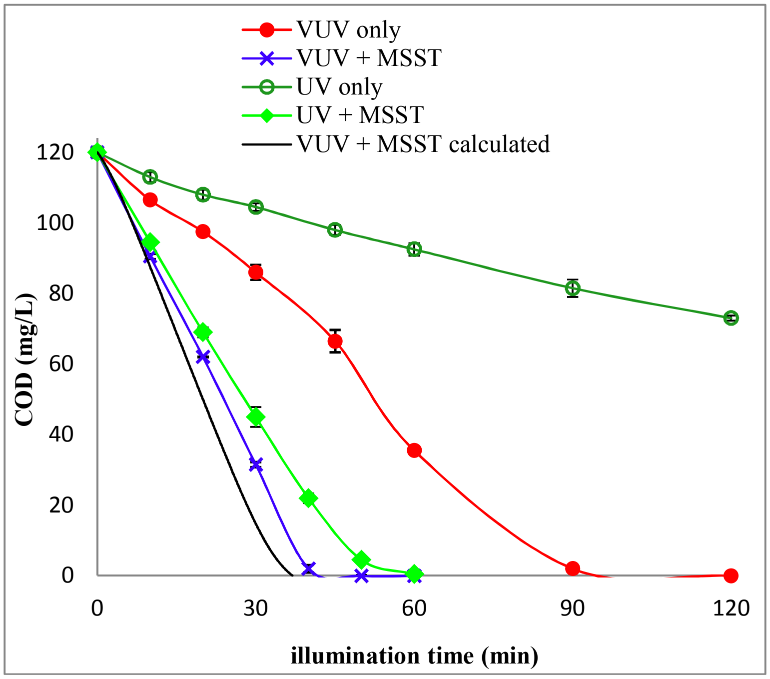

Figure 5

496

497

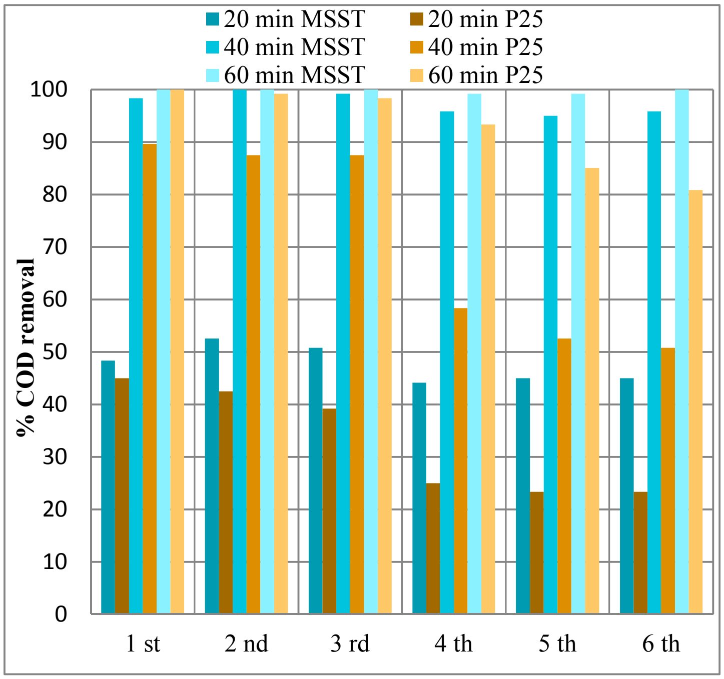

Figure 6

498

499

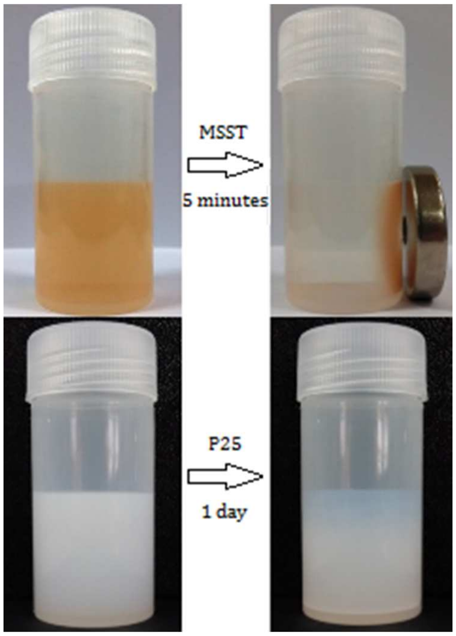

Figure 7

Table 1	
Duration of the solvothermal process (hour)	Crystalline size (nm)
3	19.4
6	19.2
12	18.2
18	16.7
24	15.9

Table 2

Experiment	E_{EM} (kWh/kg COD)
VUV-MSST	365
UV-MSST	521
VUV only	825
UV only (Estimated by extrapolation)	>10500
VUV-MSST calculated	335